

Climate-driven disturbances amplify forest drought sensitivity

Received: 16 August 2023

Accepted: 25 April 2024

Published online: 7 June 2024

 Check for updates

Meng Liu^{1,2}✉, Anna T. Trugman¹, Josep Peñuelas^{1,4,5} & William R. L. Anderegg^{1,2}

Forests are a major terrestrial carbon sink, but the increasing frequency and intensity of climate-driven disturbances such as droughts, fires and biotic agent outbreaks is threatening carbon uptake and sequestration. Determining how climate-driven disturbances may alter the capacity of forest carbon sinks in a changing climate is crucial. Here we show that the sensitivity of gross primary productivity to subsequent water stress increased significantly after initial drought and fire disturbances in the conterminous United States. Insect outbreak events, however, did not have significant impacts. Hot and dry environments generally exhibited increased sensitivity. Estimated ecosystem productivity and terrestrial carbon uptake decreased markedly with future warming scenarios due to the increased sensitivity to water stress. Our results highlight that intensifying disturbance regimes are likely to further impact forest sustainability and carbon sequestration, increasing potential risks to future terrestrial carbon sinks and climate change mitigation.

Terrestrial vegetation stores 450 Pg carbon (C) and sequesters ~1.9 PgC yr⁻¹ (ref. 1) (net carbon sink), which counterbalances approximately 20% of global carbon emissions from fossil-fuel burning. As the primary driver of the terrestrial carbon sink, forests have a key role in regulating terrestrial ecosystems and the carbon cycle. Forests in the conterminous United States (CONUS) sequester 173 TgC yr⁻¹ (ref. 2), and offset 9.7% of anthropogenic carbon emissions annually. Forest-based strategies to mitigate climate change, such as reforestation, improved forest management and avoidance of forest loss, have been proposed as potentially impactful 'nature-based climate solutions' alongside dramatic reductions in fossil-fuel emissions^{3,4}. However, disturbances that are sensitive to climate, such as droughts, fires and insect outbreaks, decrease forest productivity, increase tree mortality and decrease carbon storage, at least at short timescales^{5–8}. At regional scales and over longer timescales, changes in disturbance regimes (for example, more-frequent and/or more-severe disturbances) impair forest resistance (the capacity of the ecosystem to maintain its state and function⁹) and increase the risk of decreasing long-term carbon storage, which is crucial for mitigating climate change¹⁰. The frequency and intensity

of prevalent disturbances, particularly droughts, fires and those from biotic agents (for example, insect outbreaks), are projected to increase in response to global warming^{11–13} and will probably play a pivotal role in future forest carbon sink. Identifying the changes and dynamics of forest gross primary production (GPP) and how forests respond to environmental stressors after disturbances is paramount in systematically managing terrestrial ecosystems and effectively mitigating climate change.

Climate-driven disturbances have both direct and indirect effects on forest GPP. Direct effects often involve a concomitant decrease in GPP during disturbances. For example, the severe heat and drought event in 2003 led to a 30% decrease in ecosystem GPP in Europe¹⁴, resulting in a strong anomalous net forest carbon source. However, these direct effects are typically short-lived for droughts, with forest GPP rebounding to pre-disturbance levels within a few months to a year¹⁵. Although, if trees die during fires and insect outbreaks, forest GPP recovery may take multiple years or longer. Indirect effects refer to changes in the sensitivity of forest GPP to climate stressors after disturbances, which can persist for several years. The sensitivity of forest

¹School of Biological Sciences, University of Utah, Salt Lake City, UT, USA. ²Wilkes Center on Climate Science and Policy, University of Utah, Salt Lake City, UT, USA. ³Department of Geography, University of California, Santa Barbara, CA, USA. ⁴CREAF, Barcelona, Spain. ⁵Global Ecology Unit CREAF-CSIC-UAB, CSIC, Barcelona, Spain. ✉e-mail: meng.liu@tamu.edu

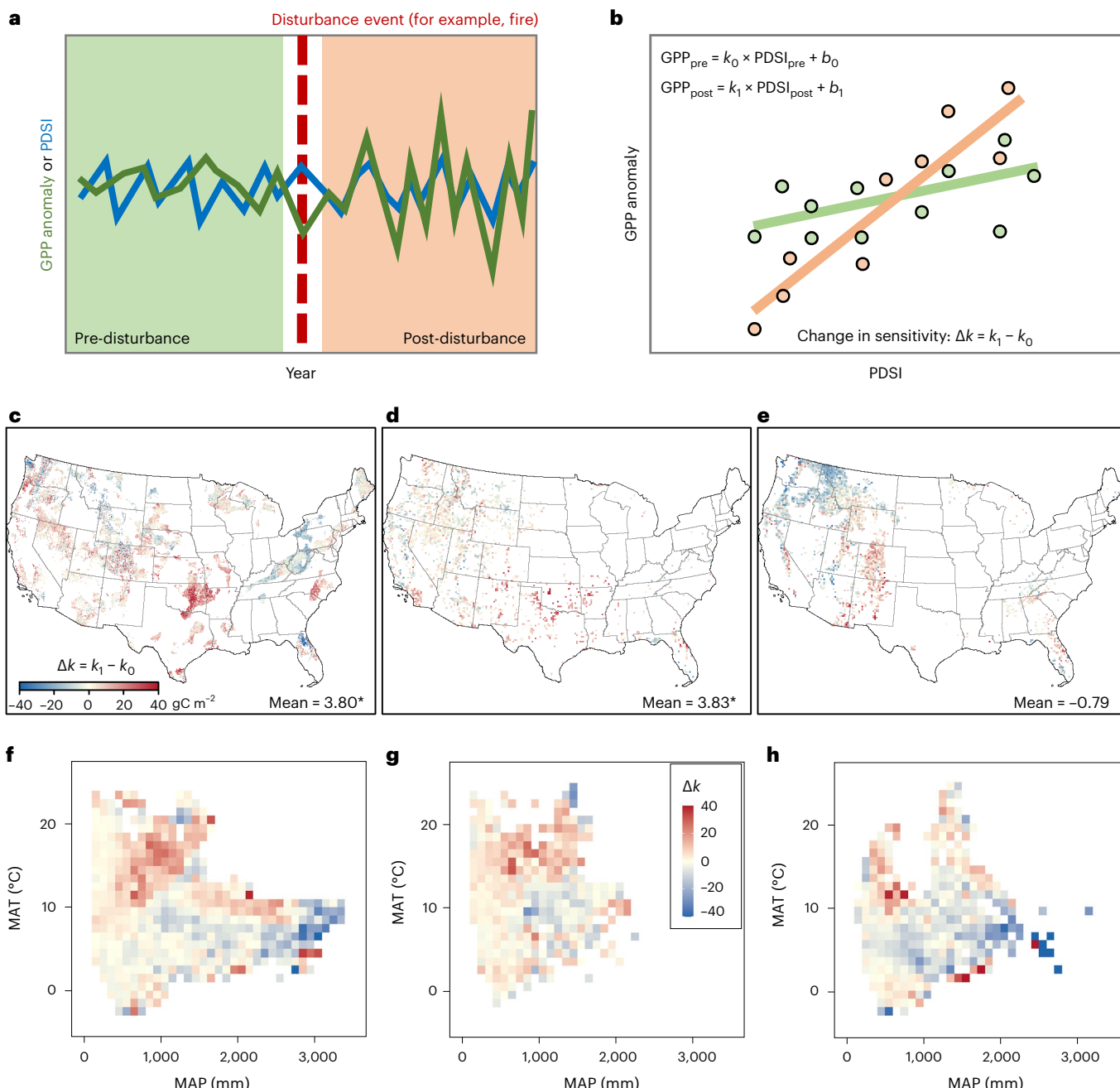


Fig. 1 | The sensitivity of GPP to water stress in CONUS changed notably after severe disturbances. **a, b**, GPP anomalies (detrended) and PDSI (a) and change in sensitivity due to disturbances (b). **c–e**, The change in sensitivity after severe drought (c), fire (d) and insect outbreak (e). Asterisks indicate significance at the 0.05 level (two-sided) based on the GLS model. Multiple comparisons are

not applicable. The distribution maps (4 km) for fires and insect outbreaks were aggregated to 20 km for visual display. **f–h**, The change in sensitivity in climate space (mean annual temperature (MAT) versus mean annual precipitation (MAP) after drought (f), fire (g) and insect outbreak (h); 1°C × 100 mm grid).

GPP to water stress, particularly water availability, is a critical measure of response that indicates the ‘resistance’ of forests to environmental variability and their capacity to sequester carbon. High sensitivity (low resistance) to water stress often signifies a high vulnerability to water deficits and climatic extremes, frequently preceding an increase in forest mortality¹⁶. The sensitivity of forest productivity, including GPP, tree-ring width, basal area growth and greenness, to drought can be influenced by various factors, such as environmental conditions (soil, topography and climate), stand composition (species and age), plant functional traits (wood density and hydraulic traits) and human management^{9,17–24}. However, a comprehensive understanding of the

indirect effects of disturbances on forest GPP is currently lacking. It remains unknown whether forest GPP becomes more or less sensitive to water stress after disturbances. Quantifying the long-term changes in the sensitivity of GPP to water stress in response to disturbances is crucial for enhancing our understanding and modelling the impacts of climate change on forest carbon cycling in the twenty-first century.

We aimed to investigate whether the sensitivity of ecosystem GPP to water stress changes after severe droughts, fires and insect outbreaks. We examined the factors driving these changes and assessed their implications for carbon uptake. Leveraging long-term remotely sensed GPP data in CONUS, we performed regression analysis to

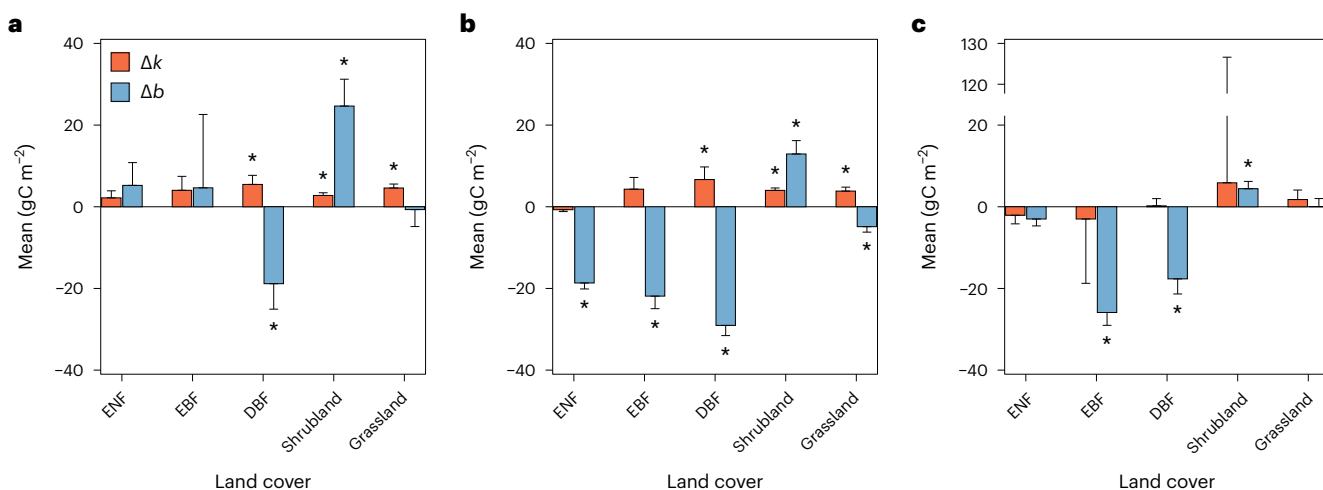


Fig. 2 | The drought sensitivity of forests increased after severe disturbances.

a–c, The mean changes in sensitivity (Δk) and intercept (Δb) for different land covers in CONUS after severe drought (left to right, $N = 2,401,414,4,691,1,127,7,719$) (a), fire ($N = 1,944,178,258,601,6,068$) (b) and insect outbreak ($N = 7,320$,

111,548,157,3,904) (c). The error bars are s.e.m., and the asterisks indicate that the mean is significant at the 0.05 level (two-sided) based on the GLS model. Multiple comparisons are not applicable. DBF, deciduous broadleaf forest; EBF, evergreen broadleaf forest; ENF, evergreen needleleaf forest.

understand the response of plant productivity to variations in water stress, as indicated by widely used drought indices such as the Palmer drought severity index (PDSI)²⁵ and the standardized precipitation–evapotranspiration index (SPEI)²⁶. We calculated the sensitivity of forest GPP to water stress (referred to as ‘drought sensitivity’) and compared it before and after disturbances. Machine-learning models, specifically random forest regression, were used to uncover the drivers and potential mechanisms underlying changes in drought sensitivity. We sought to answer the following research questions. (1) How does drought sensitivity change after severe disturbances across CONUS? (2) How do changes in drought sensitivity vary across different land-cover and ecosystem types? (3) What are the major factors influencing changes in drought sensitivity? (4) How might the observed changes in drought sensitivity affect vegetation carbon uptake under future warming scenarios?

Change in drought sensitivity at the continental scale

The drought sensitivity across CONUS changed significantly after severe droughts and fires. We illustrated how to calculate the change in GPP drought sensitivity with schematics (Fig. 1a,b). The sensitivity increased significantly after severe droughts and fires (Fig. 1c,d and Supplementary Table 1), where the means of the changes in sensitivity (Δk) were $3.80 \pm 0.95 \text{ gC m}^{-2}$ (mean \pm s.e.m.; $P = 0.0001$, generalized least squares (GLS)) and $3.83 \pm 0.73 \text{ gC m}^{-2}$ ($P = 0$, GLS), respectively. Most pixels (59.12%) indicated increased sensitivity after severe droughts, but some pixels in eastern and northwestern CONUS manifested decreased sensitivity (Fig. 1c). Fewer pixels were available for analysing the effects of fires, but the increase in sensitivity after fires was still significant (Fig. 1d), with 58.64% of the available pixels indicating increased sensitivity. The sensitivity, however, did not change significantly after insect outbreaks, $-0.79 \pm 1.23 \text{ gC m}^{-2}$ ($P = 0.52$, GLS) (Fig. 1e). Forests in the northwest had decreased sensitivity after insect outbreaks, whereas those in the Rocky Mountains had increased sensitivity. The results were similar when using SPEI to represent water stress (Extended Data Fig. 1a–c), where the sensitivity increased significantly across CONUS after severe droughts and fires, at $5.68 \pm 2.06 \text{ gC m}^{-2}$ ($P = 0.0058$, GLS) and $3.95 \pm 1.73 \text{ gC m}^{-2}$ ($P = 0.023$, GLS), respectively, and decreased significantly after insect outbreaks, $-6.22 \pm 2.73 \text{ gC m}^{-2}$ ($P = 0.022$, GLS). We note as well that the patterns were robust when considering only pixels with significant GPP–PDSI relationships (Extended

Data Fig. 2 and Supplementary Table 2). In summary, disturbances clearly altered GPP drought sensitivity, but the directions of the change in sensitivity diverged among disturbances and regions.

The sensitivity increased significantly ($\Delta k = 6.21 \pm 1.06 \text{ gC m}^{-2}$, $P = 0$, GLS; Supplementary Table 3) in hot and dry regions (for example, temperature (T) $> 10^\circ\text{C}$ and precipitation (P) $< 1,000 \text{ mm}$) (Fig. 1f) and did not change in cold and wet regions (for example, $T < 10^\circ\text{C}$ and $P > 2,000 \text{ mm}$) after severe droughts. The sensitivity increased significantly in hot and dry regions after fires ($\Delta k = 5.33 \pm 0.72 \text{ gC m}^{-2}$, $P = 0$, GLS); there were almost no wet regions (only five pixels) (Fig. 1g) because fire was concentrated in dry regions. After insect outbreaks, the sensitivity did not change in hot and dry regions and decreased significantly in cold and wet regions ($\Delta k = -28.49 \pm 6.80 \text{ gC m}^{-2}$, $P = 0.0002$, GLS) (Fig. 1h). The intercept of the GPP–PDSI model decreased significantly after disturbances, where the means of the changes in the intercept (Δb) were all significantly lower than zero: $-7.91 \pm 3.51 \text{ gC m}^{-2}$ ($P = 0.024$, GLS), $-7.73 \pm 0.90 \text{ gC m}^{-2}$ ($P = 0$, GLS) and $-7.80 \pm 1.94 \text{ gC m}^{-2}$ ($P = 0.0001$, GLS) (Extended Data Fig. 3).

Change in drought sensitivity among land-cover types

The drought sensitivity of forests generally increased after severe disturbances, with some notable differences among forest types. The sensitivity increased after severe droughts for evergreen needleleaf, evergreen broadleaf and deciduous broadleaf forests (Extended Data Fig. 4, Fig. 2a and Supplementary Table 1), with the largest increase in deciduous broadleaf forests ($5.47 \pm 2.22 \text{ gC m}^{-2}$; $P = 0.014$, GLS). Evergreen and deciduous broadleaf forests were more sensitive to water stress after fires, and evergreen needleleaf forests were less sensitive, at $-0.73 \pm 0.45 \text{ gC m}^{-2}$ (Fig. 2b). The change in the sensitivity was significant only in deciduous broadleaf forests, at $6.67 \pm 3.08 \text{ gC m}^{-2}$ ($P = 0.031$, GLS). The drought sensitivity of forests did not change after insect outbreaks. The changes in the sensitivity of shrubland and grassland were large but not always significant. The changes in drought sensitivity were highly unlikely to be due to long-term trends because undisturbed regions had different trends in sensitivity during 1982–2018 compared with disturbed regions with the same land-cover type (Extended Data Fig. 5). These results confirmed that the sensitivity of forests was affected by severe disturbances and that the sensitivity tended to increase after disturbances. The results were comparable when using SPEI (Extended Data Fig. 1d–f), where evergreen broadleaf

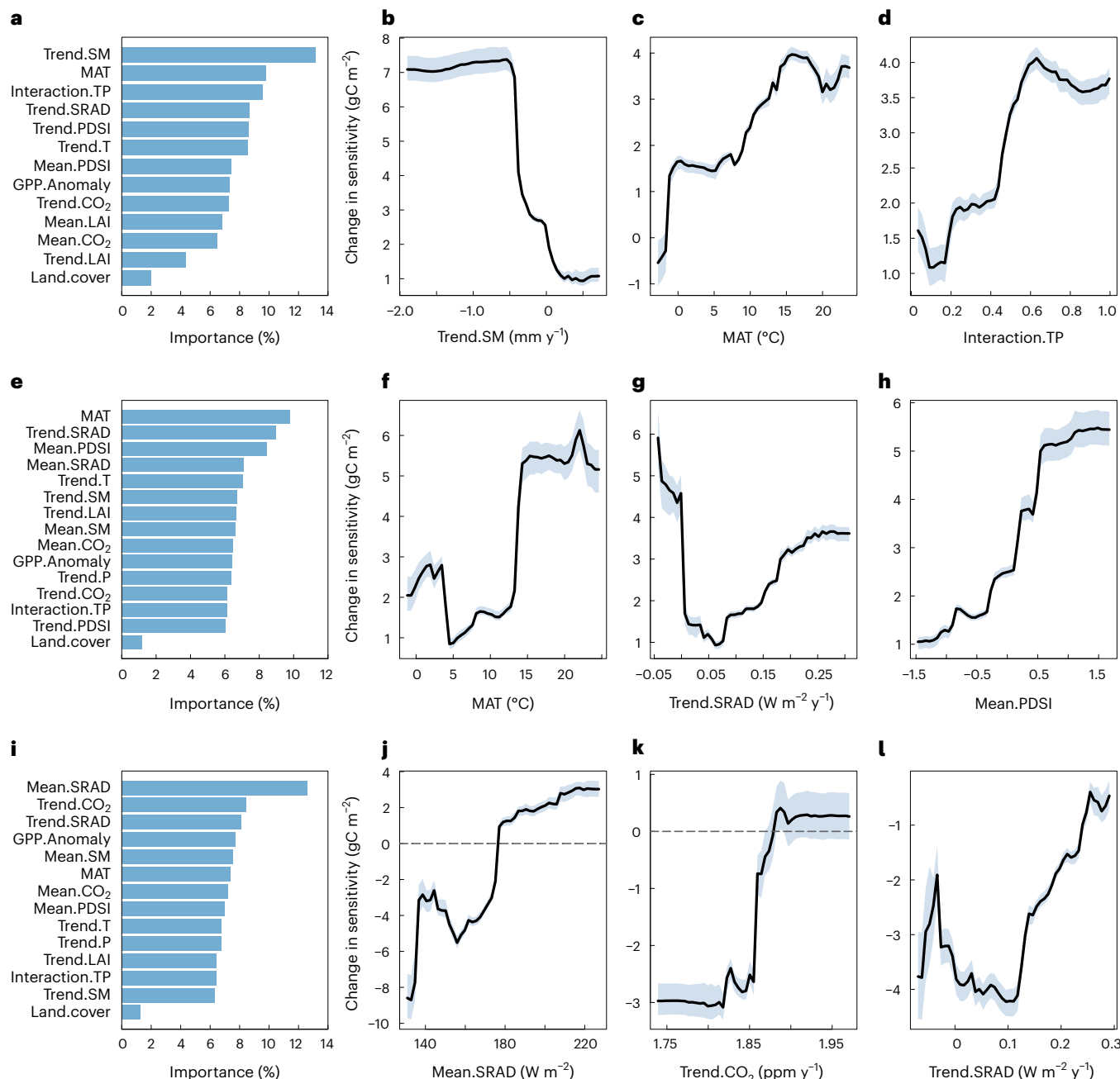


Fig. 3 | Drivers of the change in GPP drought sensitivity. **a–d**, Drivers of the change in the sensitivity of GPP to water stress after severe drought: importance of drivers (a) and random forest partial dependence of the change in sensitivity on the three most important drivers: trend of soil moisture (Trend.SM) (b), MAT (c) and the interaction between temperature and reversed precipitation (Interaction.TP) (d). **e–h**, Drivers of the change in the sensitivity of GPP to water stress after severe fire: importance of drivers (e) and random forest partial dependence of the change in sensitivity on the three most important drivers:

MAT (f), trend of SRAD (g) and mean annual PDSI (h). **i–l**, Drivers of the change in the sensitivity of GPP to water stress after severe insect outbreak: importance of drivers (i) and random forest partial dependence of the change in sensitivity on the three most important drivers: mean annual SRAD (j), trend of CO₂ (k) and trend of SRAD (l). The solid black line is the average, and the shading shows the range (from minimum to maximum) of the partial dependence from 100 runs of random forest models. LAI, leaf area index.

and deciduous broadleaf forests exhibited significantly increased sensitivity, at $23.50 \pm 8.14 \text{ gC m}^{-2}$ ($P = 0.0041$, GLS) and $16.18 \pm 7.04 \text{ gC m}^{-2}$ ($P = 0.022$, GLS), after severe droughts.

The intercept of the GPP–PDSI model decreased in forests (Fig. 2 and Supplementary Table 1). The decreases were due to lower biomass and foliar area caused by disturbances, leading to decreased forest productivity. The directions of the changes in the intercept were not consistent for grassland and shrubland. It is very intriguing that the

intercept of shrubland increased after all three disturbances, which might indicate that the direct effects (GPP decrease) of disturbances on shrubland can recover quickly. However, the intercept change is not related strictly to the absolute GPP change since we used detrended GPP. From the perspective of vegetation structure, shrubs have smaller leaf area, frequent resprouting behaviours and shorter canopy heights than forests, which might benefit the recovery of shrubland productivity after disturbances.

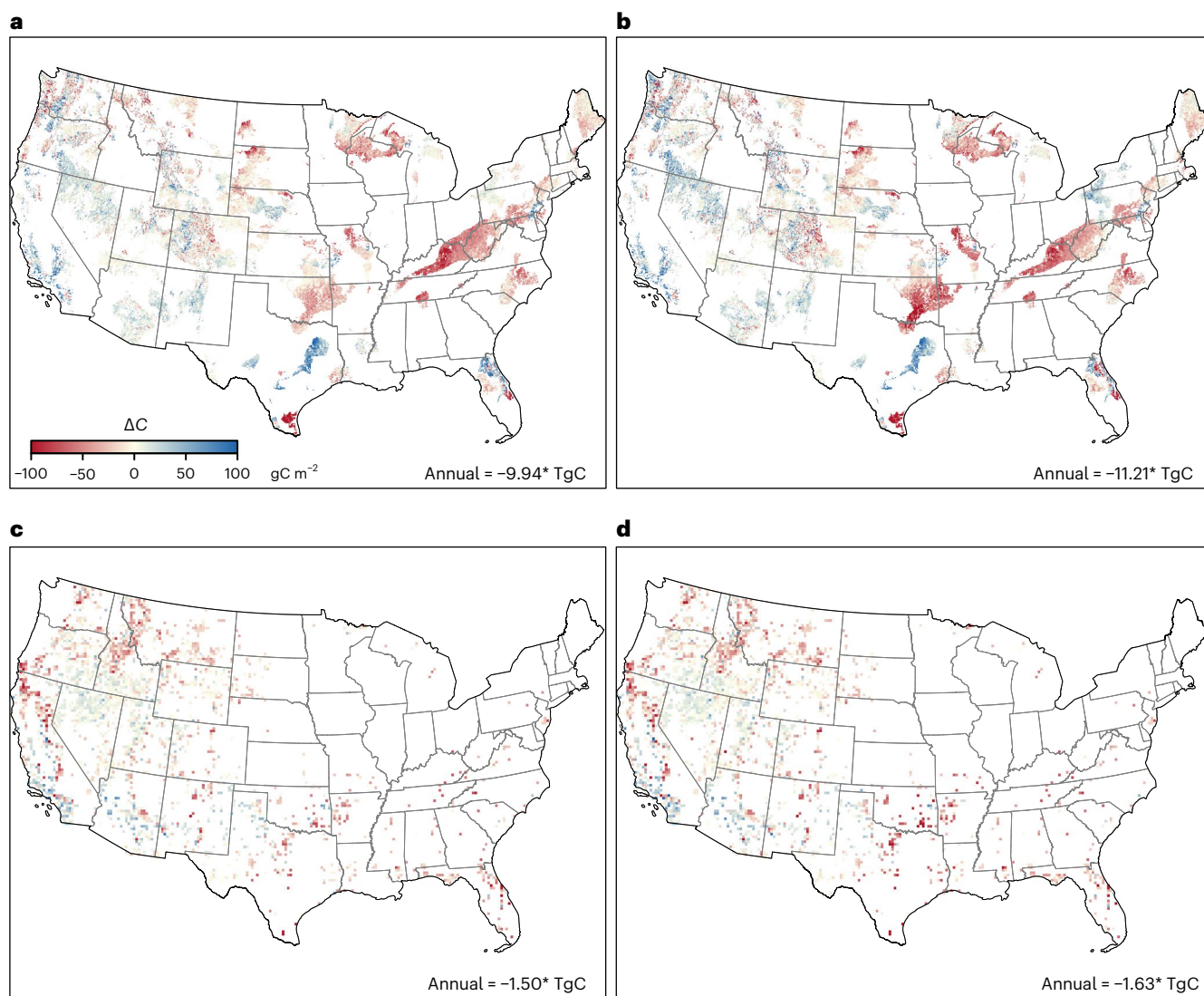


Fig. 4 | Carbon uptake decreases in warming scenarios. **a,b**, The average change in carbon uptake (ΔC) due to the change in sensitivity after severe drought under historical time (**a**) and $+2^{\circ}\text{C}$ warming scenario (**b**). **c,d**, The average ΔC due to the change in sensitivity after severe fire under historical time

(**c**) and $+2^{\circ}\text{C}$ warming (**d**). ‘Annual’ indicates mean annual total ΔC across CONUS, and the asterisk indicates the mean is significant at the 0.05 level (two-sided, both GLS models and *t* test). Multiple comparisons are not applicable. Panels **c** and **d** are aggregated to 20 km for visual display.

Factors influencing the change in drought sensitivity

Several climatic factors play a crucial role in driving the change in drought sensitivity. These factors include the trend of soil moisture, mean annual temperature, the interaction between temperature and reversed precipitation and downward surface short-wave radiation (SRAD). For drought, the random forest model explained 67% of the variation ($R^2 = 0.67$; Extended Data Fig. 6a) in the change in sensitivity, with the trend of soil moisture emerging as the most important driver (Fig. 3a). Mean annual temperature and the interaction between temperature and reversed precipitation ranked as the second and third most important drivers, respectively. The change in sensitivity increased with decreasing trends of soil moisture (Fig. 3b), indicating that lower soil moisture levels contributed to higher post-disturbance sensitivity. Similarly, the change in sensitivity increased with mean annual temperature (Fig. 3c), suggesting that regions experiencing higher temperatures were more likely to exhibit increased sensitivity after disturbances. The interaction between temperature and reversed precipitation (Fig. 3d) had similar effects to mean annual temperature,

with higher values (indicating hot and dry regions) associated with increased drought sensitivity.

For fires and insect outbreaks, the random forest models explained 37% and 28% of the variations in sensitivity change, respectively (Extended Data Fig. 6b,c). Mean annual temperature emerged as the most important driver for fires (Fig. 3e), where regions with higher temperatures were associated with increases in sensitivity after the disturbance (Fig. 3f), particularly when mean annual temperature exceeded approximately 15°C . Increasing, increasing downward surface short-wave radiation (particularly when the trend of SRAD is greater than zero) and a high PDSI were linked to an increase in sensitivity after fires. In the case of insect outbreaks, mean annual downward surface short-wave radiation emerged as the most important driver (Fig. 3i), with regions experiencing high radiation (for example, $>180 \text{ W m}^{-2}$) demonstrating increased sensitivity, whereas regions with low radiation exhibited decreased sensitivity after the disturbance (Fig. 3j). This result aligns with the distribution of sensitivity change after insect outbreaks (Fig. 1e), where northwest regions generally displayed decreased sensitivity and low levels of short-wave radiation.

Increasing trends in CO₂ and short-wave radiation also contributed to the increase in sensitivity after insect outbreaks (Fig. 3k,l).

Effects on carbon uptake

The change in drought sensitivity of GPP has notable implications for carbon uptake and loss. We quantified carbon uptake responses to water stress and assessed the recovery time by utilizing pixels with a post-disturbance period of at least 16 years (Methods). It took approximately 5 years for the sensitivity to return to the pre-disturbance level after severe droughts and around 6 years after fires (Extended Data Fig. 7b,c). Owing to the relatively short post-disturbance time (9 years: 2010–2018), the recovery time for insect outbreaks was not calculated. We further estimated the potential change in carbon uptake resulting from the sensitivity change. As a first-order exploration, the change in carbon uptake was calculated as the difference in GPP when considering the changes in sensitivity and intercept (equation (2)). For drought, the mean annual change in carbon uptake over the 5 year period following the disturbance was -9.94 ± 2.99 TgC (Fig. 4a) across CONUS, indicating a reduction in carbon absorption. For fires, the mean annual change in carbon uptake over the 6 year period after the disturbance was -1.50 ± 0.03 TgC (Fig. 4c). To assess the effects of future warming, PDSI under the +2 °C warming scenario was used to estimate the change in carbon uptake in response to the sensitivity change. For drought, the change in carbon uptake under the +2 °C warming scenario was estimated to be -11.21 ± 2.42 TgC (Fig. 4b), indicating even lower carbon absorption than historical conditions. For fires, the change in carbon uptake was estimated to be -1.63 ± 0.04 TgC under the warming scenario (Fig. 4d).

Implications for climate change mitigation

Severe disturbances, such as severe droughts, fires and insect outbreaks, have substantial effects on forest ecosystems. They all have the potential to alter forest composition, leading to a shift towards early succession species²⁷, and can cause physiological damage to surviving trees. Both effects influence the sensitivity of post-disturbance forest productivity to water availability. This study specifically examines the indirect effects of severe disturbances and highlights the changes in GPP drought sensitivity following these extreme events. We have observed that severe disturbances, such as severe droughts and fires, tend to increase the sensitivity of forest productivity to water availability. This is particularly notable in deciduous broadleaf forests, possibly due to drought legacy effects²⁸ and disturbance-induced damage, such as embolism and overheating. These factors make trees more susceptible to subsequent water stress. In addition, for deciduous trees, physiological traits such as shallow roots²⁹ and thin bark probably contribute to increased susceptibility to fire and drought damage. By contrast, for evergreen needleleaf forests, the sensitivity did not change and even decreased after fires and insect outbreaks. This phenomenon may be attributed to decreases in stand density following disturbances. In general, stand density has increased in many evergreen needleleaf forests in the western USA due to historical fire suppression activities³⁰. Disturbances can relax overstocked conditions and reduce competition³¹ for water. This result suggests that thinning holds the potential to alleviate water stress in certain conifer forests. In addition, gymnosperm-dominated forests, mainly needleleaf forests in the western USA, have shown notable shifts characterized by decreases in P50 (water potential at which 50% of conductivity is lost) and increases in the hydraulic safety margin (that is, the difference between P50 and the minimum water potential experienced)³² in response to climate-driven mortality, making these forests more drought tolerant.

Non-forested ecosystems, such as shrublands and grasslands, also exhibit heightened drought sensitivity following disturbances, especially after severe droughts and fires. This increased sensitivity may be attributed to their proximity to absolute biogeographic and

climate thresholds. Shrubs and grasses predominantly thrive in arid regions characterized by high solar radiation and temperature coupled with low water availability. Moreover, dry regions, particularly shrublands and grasslands, reveal stronger correlations between GPP and PDSI (Extended Data Fig. 2b). Climate emerges as a crucial factor influencing sensitivity changes, with hot and dry regions experiencing increased sensitivity and cold and wet regions showing decreased sensitivity (Fig. 1). Previous research²⁸ also indicates that plants in arid regions exhibit stronger drought legacy effects compared with those in wet regions.

Droughts, fires and insect outbreaks have varied effects on ecosystems. In general, understory species such as grasses and herbs are sensitive to water availability³³ and usually senesce rapidly due to water deficits. During droughts, both the understory and overstory vegetation will be constrained. The absolute GPP values of understory grasses might recover in the next year; however, the GPP sensitivity to water (indirect effects) of the whole ecosystem, including both the understory and overstory vegetation, may not recover as quickly. The sensitivity of grasslands increased significantly ($P=0$, GLS) after droughts (Fig. 2a), indicating that the GPP sensitivity of grasses may not necessarily recover at the same pace as the absolute GPP. For overstory trees, drought legacy effects can last for years²⁸. A similar situation goes for fires, where both the understory grasses and overstory trees might be burned during fires. The absolute GPP of understory grasses can recover quickly; however, the GPP sensitivity might not (Fig. 2b). For overstory trees, fire damage, such as heat stress (for example, heat emboli) and biomass consumption, can cause a long-lasting sensitivity change. For insect outbreaks, understory grasses are not the target of widespread insects such as bark beetles⁷, and thus the impacts of insects on understory vegetation will be small. The unchanged (or even decreased) sensitivity after insect outbreaks could be due to the decreases in stand density and shifts in composition.

Across CONUS, the increased sensitivity of GPP to water stress leads to substantial decreases in carbon uptake after severe droughts and fires. These decreases are logical as photosynthesis and carbon uptake tend to decline more when sensitivity increases at the same level of water stress, and climate change is likely to bring more-frequent and severe droughts in many regions. Our estimates suggest that the decrease in carbon uptake can persist for approximately 5–6 years after the disturbances. This reduction in carbon uptake hampers the capacity of terrestrial ecosystems to sequester anthropogenic carbon emissions. Furthermore, our findings highlight the accelerated decline in carbon uptake under warming scenarios. Less carbon would be absorbed in response to increased sensitivity under warming scenarios compared with historical conditions. Many regions in CONUS are projected to experience hotter and drier conditions under future warming scenarios¹³, leading to increased water stress on plant growth. As a result, ecosystems' ability to absorb carbon would decline, exacerbated by increased water stress and vegetation sensitivity. Regions such as western North America face high risks of carbon loss and species loss due to climate change, as indicated by global assessments³⁴.

Climate change is expected to increase the frequency and severity of disturbances in many regions. From the perspective of climate policy and management, relying on planting more trees to counterbalance carbon emissions from fossil-fuel burning can be challenging, particularly when ecosystem productivity is threatened by disturbances that are climate dependent. Our results highlight pervasive changes in the drought sensitivity of GPP in forests after disturbances and indicate meaningful effects on carbon uptake. Increased sensitivity increases the vulnerability of ecosystems to drought and could lead to substantial decreases in ecosystem carbon uptake under future warming scenarios. These long-term dynamics are important for evaluating the capacity of terrestrial ecosystems as carbon sinks for carbon management, nature-based climate solutions and net-zero pledges.

Online content

Any methods, additional references, Nature Portfolio reporting summaries, source data, extended data, supplementary information, acknowledgements, peer review information; details of author contributions and competing interests; and statements of data and code availability are available at <https://doi.org/10.1038/s41558-024-02022-1>.

References

1. Friedlingstein, P. et al. Global carbon budget 2022. *Earth Syst. Sci. Data* **14**, 4811–4900 (2022).
2. Wear, D. N. & Coulston, J. W. From sink to source: regional variation in US forest carbon futures. *Sci. Rep.* **5**, 16518 (2015).
3. Griscom, B. W. et al. Natural climate solutions. *Proc. Natl Acad. Sci. USA* **114**, 11645–11650 (2017).
4. Fargione, J. E. et al. Natural climate solutions for the United States. *Sci. Adv.* **4**, eaat1869 (2018).
5. Seidl, R. et al. Forest disturbances under climate change. *Nat. Clim. Change* **7**, 395–402 (2017).
6. McDowell, N. G. & Allen, C. D. Darcy's law predicts widespread forest mortality under climate warming. *Nat. Clim. Change* **5**, 669–672 (2015).
7. Williams, C. A., Gu, H., MacLean, R., Masek, J. G. & Collatz, G. J. Disturbance and the carbon balance of US forests: a quantitative review of impacts from harvests, fires, insects, and droughts. *Glob. Planet. Change* **143**, 66–80 (2016).
8. Hemes, K. S., Norlen, C. A., Wang, J. A., Goulden, M. L. & Field, C. B. The magnitude and pace of photosynthetic recovery after wildfire in California ecosystems. *Proc. Natl Acad. Sci. USA* **120**, e2201954120 (2023).
9. Anderegg, W. R. L., Trugman, A. T., Badgley, G., Konings, A. G. & Shaw, J. Divergent forest sensitivity to repeated extreme droughts. *Nat. Clim. Change* **10**, 1091–1095 (2020).
10. Anderegg, W. R. L. et al. Climate-driven risks to the climate mitigation potential of forests. *Science* **368**, eaaz7005 (2020).
11. Anderegg, W. R. L. et al. Future climate risks from stress, insects and fire across US forests. *Ecol. Lett.* **25**, 1510–1520 (2022).
12. Dai, A. Drought under global warming: a review. *Wiley Interdiscip. Rev. Clim. Change* **2**, 45–65 (2011).
13. Cook, B. I., Ault, T. R. & Smerdon, J. E. Unprecedented 21st century drought risk in the American Southwest and Central Plains. *Sci. Adv.* **1**, e1400082 (2015).
14. Ciais, P. et al. Europe-wide reduction in primary productivity caused by the heat and drought in 2003. *Nature* **437**, 529–533 (2005).
15. Schwalm, C. R. et al. Global patterns of drought recovery. *Nature* **548**, 202–205 (2017).
16. Keen, R. M. et al. Changes in tree drought sensitivity provided early warning signals to the California drought and forest mortality event. *Glob. Change Biol.* **28**, 1119–1132 (2022).
17. Fu, Z. et al. Sensitivity of gross primary productivity to climatic drivers during the summer drought of 2018 in Europe. *Phil. Trans. R. Soc. B* **375**, 20190747 (2020).
18. Phillips, R. P. et al. A belowground perspective on the drought sensitivity of forests: towards improved understanding and simulation. *For. Ecol. Manage.* **380**, 309–320 (2016).
19. McDowell, N. et al. Mechanisms of plant survival and mortality during drought: why do some plants survive while others succumb to drought? *N. Phytol.* **178**, 719–739 (2008).
20. Cartwright, J. M., Littlefield, C. E., Michalak, J. L., Lawler, J. J. & Dobrowski, S. Z. Topographic, soil, and climate drivers of drought sensitivity in forests and shrublands of the Pacific Northwest, USA. *Sci. Rep.* **10**, 18486 (2020).
21. Rosner, S. et al. Wood density as a screening trait for drought sensitivity in Norway spruce. *Can. J. For. Res.* **44**, 154–161 (2014).
22. Mausolf, K. et al. Higher drought sensitivity of radial growth of European beech in managed than in unmanaged forests. *Sci. Total Environ.* **642**, 1201–1208 (2018).
23. Lebourgeois, F., Gomez, N., Pinto, P. & Mérian, P. Mixed stands reduce *Abies alba* tree-ring sensitivity to summer drought in the Vosges mountains, western Europe. *For. Ecol. Manage.* **303**, 61–71 (2013).
24. Linares, J. C., Taïqui, L., Sangüesa-Barreda, G., Seco, J. I. & Camarero, J. J. Age-related drought sensitivity of Atlas cedar (*Cedrus atlantica*) in the Moroccan Middle Atlas forests. *Dendrochronologia* **31**, 88–96 (2013).
25. Palmer, W. C. *Meteorological Drought* (US Department of Commerce Weather Bureau, 1965).
26. Beguería, S., Vicente-Serrano, S. M., Reig, F. & Latorre, B. Standardized precipitation evapotranspiration index (SPEI) revisited: parameter fitting, evapotranspiration models, tools, datasets and drought monitoring. *Int. J. Climatol.* **34**, 3001–3023 (2014).
27. Trugman, A. T., Medvigy, D., Anderegg, W. R. L. & Pacala, S. W. Differential declines in Alaskan boreal forest vitality related to climate and competition. *Glob. Change Biol.* **24**, 1097–1107 (2018).
28. Anderegg, W. R. L. et al. Pervasive drought legacies in forest ecosystems and their implications for carbon cycle models. *Science* **349**, 528–532 (2015).
29. Tumber-Dávila, S. J., Schenk, H. J., Du, E. & Jackson, R. B. Plant sizes and shapes above and belowground and their interactions with climate. *N. Phytol.* **235**, 1032–1056 (2022).
30. Voelker, S. L. et al. Fire deficits have increased drought sensitivity in dry conifer forests: fire frequency and tree-ring carbon isotope evidence from Central Oregon. *Glob. Change Biol.* **25**, 1247–1262 (2019).
31. Sheil, D. Disturbance and distributions: avoiding exclusion in a warming world. *Ecol. Soc.* **21**, 445–466 (2016).
32. Trugman, A. T., Anderegg, L. D. L., Shaw, J. D. & Anderegg, W. R. L. Trait velocities reveal that mortality has driven widespread coordinated shifts in forest hydraulic trait composition. *Proc. Natl Acad. Sci. USA* **117**, 8532–8538 (2020).
33. Adhikari, A. et al. Management and climate variability effects on understory productivity of forest and savanna ecosystems in Oklahoma, USA. *Ecosphere* **12**, e03576 (2021).
34. Anderegg, W. R. L. et al. A climate risk analysis of Earth's forests in the 21st century. *Science* **377**, 1099–1103 (2022).

Publisher's note Springer Nature remains neutral with regard to jurisdictional claims in published maps and institutional affiliations.

Springer Nature or its licensor (e.g. a society or other partner) holds exclusive rights to this article under a publishing agreement with the author(s) or other rightsholder(s); author self-archiving of the accepted manuscript version of this article is solely governed by the terms of such publishing agreement and applicable law.

© The Author(s), under exclusive licence to Springer Nature Limited 2024

Methods

Data

We used GPP to indicate the photosynthetic capacity and productivity of forests. Four state-of-the-art long-term GPP datasets covering CONUS were used: the Numerical Terradynamic Simulation Group (NTSG) Landsat GPP dataset³⁵, the Global Land Surface Satellite (GLASS) GPP dataset³⁶, the revised Eddy Covariance–Light Use Efficiency (EC-LUE) model-derived GPP dataset³⁷ and the near-infrared reflectance of vegetation (NIRv)-based GPP dataset³⁸. The Numerical Terradynamic Simulation Group Landsat GPP dataset (1986–2021) provided 16 day 30 m GPP data based on Landsat data and climatic variables across CONUS. (See Supplementary Information for details on these GPP products.) The four sets of GPP data were resampled to 4 km and aggregated to the annual level. Anomalies were calculated and detrended for each pixel for each GPP product. The four detrended anomalies were averaged for each pixel for all subsequent analysis to avoid inconsistencies and biases among the GPP products. The following analysis was based on the average anomalies of the four GPP products from 1982 to 2018.

We utilized two widely recognized drought indices, the PDSI^{25,39} and the SPEI²⁶, to quantify water stress and calculate changes in GPP drought sensitivity. The PDSI is a standardized metric derived from a two-layer soil–water balance model, where negative values indicate dry conditions and positive values indicate wet conditions. We obtained monthly historical PDSI data at a 4 km resolution covering the period between 1982 and 2018 from TerraClimate⁴⁰, which provides climatic variables such as temperature, precipitation, soil moisture, potential evapotranspiration (PET) and downward surface SRAD. The PDSI data from TerraClimate were based on the Penman–Monteith equation-based PET. Monthly PDSI values were averaged to generate annual PDSI data. Severe drought disturbances were defined as annual PDSI values below -3 (refs. 25,41). Other thresholds such as -2 and -4 were also tested, and the results were comparable when using -3 and -4 . The -2 threshold usually indicates moderate droughts, which have limited effects on ecosystems. The SPEI is a multi-scalar drought index that captures atmospheric water deficits by considering the difference between precipitation and PET. In our analysis, we used monthly precipitation and PET data from TerraClimate at a 4 km resolution to calculate the monthly 4 km SPEI12 (scale = 12 months) between 1982 and 2018 using the ‘SPEI’ package in R. SPEI12 was selected as we used annual data in this study. Monthly SPEI12 values were averaged to the annual level, and severe droughts were defined as SPEI12 values below -1.2 (ref. 9). Other thresholds such as -1 and -1.5 were also tried, and the results were comparable when using -1.2 and -1.5 . The -1 threshold is usually related to moderate droughts, which have limited effects on ecosystems.

Maps of annual fire severity were obtained from the Monitoring Trends in Burn Severity (MTBS) database, which has provided fire maps for the USA since 1984. The 30 m resolution maps of annual fire severity between 1984 and 2018 were downloaded and aggregated to 4 km. Low-severity pixels were discarded because low-severity fires generally have very small effects on forests. The proportion of burned 30 m pixels (moderate- and high-severity pixels) within each 4 km grid was calculated when aggregating the 30 m pixels to 4 km data. A 4 km grid was treated as burned when the proportion was $>10\%$. Plots from the Forest Inventory and Analysis (FIA) programme were used to identify damage caused by insect outbreaks. Agent codes of 10–19 for the FIA plots indicate that insects caused mortality. The rates of mortality of basal area due to insects were used to indicate insect damage. The mean annual rate of mortality for each plot during 2000–2009 was taken from ref. 11. We aggregated the plots to 4 km and calculated the average rate for each pixel. An average rate $>0.3\%$ was used to define insect outbreaks. The species of biotic agents (particularly insects here) were not provided by the FIA data.

Land-cover maps at a resolution of 500 m from the Terra and Aqua combined MODIS (Moderate Resolution Imaging Spectroradiometer)

Land Cover Type (MCD12Q1) version 6 from 2001 to 2020 were used to identify different vegetation types. Land-cover type 5 was used, where croplands and non-vegetation (water, urban and barren) classes were removed. Pixels with changes in land cover in 2001–2020 were also removed. We aggregated the 500 m land-cover maps to 4 km to match the GPP data. The land-cover map for 2001 is shown in Extended Data Fig. 4.

Analysis of sensitivity

The slope of a linear regression (GPP anomaly versus PDSI) was used to represent the sensitivity of photosynthesis to water availability because most pixels ($\sim 70\%$) in CONUS presented a linear relationship between GPP anomaly and PDSI (Extended Data Fig. 2). Those pixels presenting nonlinear relationships were dominated by grasslands. Thus, although a minority of areas do not have linear GPP–PDSI relationships, our results are robust to including only significant linear relationship pixels (Extended Data Fig. 2d–f and Supplementary Table 2), and a linear model represents the most parsimonious, comparable and understandable model of drought sensitivity; thus, we used it for all analyses. We compared simple linear regression and multiple linear regression when deriving the sensitivity of GPP to water stress, where the sensitivity from the two models was significantly correlated (Extended Data Fig. 8). For droughts, the slope of the linear regression between pre-drought GPP anomalies and PDSI was calculated to indicate pre-drought sensitivity (k_0). Similarly, post-drought sensitivity (k_1) was calculated using post-drought GPP anomalies and PDSI. The difference between the post-drought and pre-drought slopes was treated as the change in sensitivity (Δk).

$$\begin{aligned} \text{GPP}_{\text{anom}} &= k_0 \times \text{PDSI} + b_0 \\ \text{GPP}_{\text{anom}} &= k_1 \times \text{PDSI} + b_1 \\ k &= k_1 - k_0, \quad b = b_1 - b_0 \end{aligned} \quad (1)$$

where b_0 and b_1 are intercepts. The change in sensitivity derived with SPEI12 was calculated in the same way shown in equation (1), where SPEI12 was used to indicate water stress.

We required at least 8 years of data for regression when calculating the slopes. According to the histogram of drought return intervals in Extended Data Fig. 9a, eight was the first break point for drought return intervals, and the disturbance return intervals of most pixels are higher than 8 years. We also tried 6 years (the trough) and 10 years (the second break point) as the minimum for regression, and the corresponding changes in sensitivity, which are comparable to the change in sensitivity (Δk) in Fig. 2a, are shown in Extended Data Fig. 9c,d. A threshold of 8 years strikes a reasonable balance between sample size and stability. A lower threshold, such as 6 years, could make the results of linear regression unstable, whereas a higher threshold would decrease the sample size. For fire (Extended Data Fig. 9b), the return intervals of most pixels were greater than 10 years, indicating that any values lower than or equal to ten were acceptable. Therefore, using eight as the minimum number of years for regression was reasonable. The length of pre-disturbance and post-disturbance data could vary, and 8 years was the minimum we used for regression analysis. The first drought was checked for each pixel. The change in sensitivity was calculated when we had at least eight data points for a regression analysis before and after the first drought. Otherwise, the second drought would be checked. This pixel was discarded if all droughts were not qualified for calculating the change in sensitivity. Continuous droughts were treated as one drought when calculating the change in sensitivity. When there were two or more drought events suitable for calculating Δk , the first one would be used. The same procedure was applied to fires, producing the change in sensitivity after a fire. For insect outbreaks, we calculated the slope between GPP anomalies and PDSI before 2000 to represent pre-outbreak sensitivity, and the slope after 2009 was treated as the

post-outbreak sensitivity. We resorted to this approximation due to the limited availability of standardized FIA plots, which were accessible only from 2000 onwards and repeated every 5 or 10 years. Although the strategy used to calculate the change in sensitivity for insect outbreaks may not be ideal, it was a reasonable approach given the data constraints. To validate our findings, we conducted a sensitivity analysis by separately analysing the four GPP anomalies and the PDSI data. The results (Extended Data Fig. 10) are comparable to those obtained using the average anomalies of the four GPP products. The sensitivity change of each land-cover type based on a single GPP product is presented in Supplementary Table 4.

To account for spatial autocorrelations in the changes in sensitivity (Δk) and intercept (Δb), we used the GLS model⁴² and examined their significance. We utilized the `gls` function from the `nlme` package in R. The exponential correlation structure, `corExp`, was selected to assess the significance of the mean Δk and mean Δb by fitting GLS models with the formulas ' $\Delta k - 1$ ' and ' $\Delta b - 1$ ' (regression with only the constant term), respectively. We experimented with five correlation structures: exponential, sphere, Gaussian, ratio and linear. The exponential correlation structure was always ranked in the top two correlation structures for minimizing Akaike information criterion. So to save time for computation (GLS models are extremely time-consuming when dealing with large samples), we decided to use the exponential correlation structure throughout the manuscript. Owing to computational intensity, we aggregated the Δk and Δb maps for drought disturbances using a factor of three (4 km to 12 km) during the calculation. If the *P* value (two-sided) was below 0.05 based on the GLS, the constant term (mean Δk or mean Δb) was considered significant.

Random forest model

We used random forest regression⁴³, a widely used machine-learning model, to capture the change in sensitivity (equation (1)) and identify the primary drivers responsible for this change. Random forest regression, which utilizes an ensemble of decision trees, is well suited for analysing high-dimensional data, such as large sample sizes with numerous predictors and complex structure. To train the random forest model, we utilized the '`randomForest`' package in R. The response variable was Δk , and the predictors included various variables: T , P , soil moisture, downward surface SRAD, PDSI, leaf area index⁴⁴ and CO_2 concentration⁴⁵. For each pixel, we calculated the long-term mean (for example, mean annual temperature) and trend (for example, the trend of temperature, which is the slope of linear regression between T and year) of these variables using data from 1982 to 2018. In addition, we incorporated the interaction between T and P as a predictor, which represented the mean quantiles of T and reversed P . First, we calculated the quantiles (0–1) of T , and high T had high quantiles. Second, we reversed P by multiplying by $-1(-1 \times P)$ and calculated the quantiles of the reversed P . Finally, we averaged the quantiles of T and reversed P . The average quantiles can represent the interaction between T and P , where high quantiles indicate hot and dry conditions. GPP anomalies in the disturbed years and land-cover types were also included as extra predictors. Before training the models, highly correlated predictors were removed. For example, when mean annual precipitation and mean annual soil moisture exhibited a high correlation ($|r| > 0.7$), the predictor with a lower correlation with Δk was eliminated. In the random forest models, we used 500 decision trees, and the number of splits was determined as the square root of the number of selected predictors ($\lfloor \sqrt{n} \rfloor$). The leaf area index data were obtained from the half-month 8 km Global Inventory Modeling and Mapping Studies LAI4g product (1982–2020)⁴⁴, which were resampled (bilinear) to 4 km and averaged to the annual level. Similarly, the global monthly 1° historical CO_2 concentration data⁴⁵ from 1982 to 2013 were resampled (bilinear) to 4 km and averaged to the annual level. Separate random forest models were developed for each of the three disturbances, as the drivers varied

among them. The resulting partial dependence plots generated by the random forest models illustrated the relationships between Δk and the predictors. Predictor importance was assessed on the basis of the decrease in node purity, where the importance of a predictor was calculated as the decrease in node purity attributed to that predictor divided by the sum of the decrease in node purity for all predictors, multiplied by 100%. We ran the random forest models 100 times and averaged the responses (importance and partial dependence) of the 100 models (Fig. 3).

Recovery time and carbon uptake change

Recovery time was determined as the duration required for the sensitivity to return to its pre-disturbance level. Because the sensitivity could increase following disturbances, ecosystems may take years to recover their original states. To derive the recovery time, we selected pixels with a post-disturbance time of at least 16 years, ensuring a minimum of two independent 8 year periods to calculate sensitivity. A moving-window strategy, utilizing 8 year intervals, was used to compute post-disturbance sensitivity for each selected pixel. Within each moving window (1–8 years, 2–9 years, 3–10 years and so on), the sensitivity was determined as the slope of linear regression between GPP anomaly and PDSI. We considered ecosystems to have recovered when the post-disturbance sensitivity was equal to or lower than the pre-disturbance sensitivity (k_0). The recovery time was defined as the first year of the moving window when the post-disturbance sensitivity was $\leq k_0$. The calculation of recovery time is illustrated in the schematic provided in Extended Data Fig. 7a, which exemplifies a recovery time of 5 years. If the sensitivity decreased after disturbances, the recovery time would be identified when the post-disturbance sensitivity was $\geq k_0$. The average recovery times for severe droughts and fires were 4.8 and 5.6 years, respectively. However, the recovery time for insect outbreaks could not be determined due to the limited post-disturbance period of 9 years (2010–2018).

The change in carbon uptake was estimated on the basis of the change in GPP. The following equation represents the change in GPP (ΔGPP) in response to the change in sensitivity after disturbances:

$$\Delta \text{GPP} = k \times \Delta k + b \quad (2)$$

where ΔGPP indicates the change in productivity, and Δk and Δb represent the changes in sensitivity and intercept, respectively (as shown in Fig. 1 and Extended Data Fig. 3). Historical PDSI data after disturbances were used to derive the change in carbon uptake ($\Delta C = \Delta \text{GPP}$). For severe droughts, the closest integer to 4.8 (5 years) was used, whereas for severe fires, the closest integer to 5.6 (6 years) was used. Each pixel was associated with five PDSI values after severe droughts and six PDSI values after severe fires, which were inputted into equation (2) to calculate the corresponding ΔC . For example, if a severe drought occurred in the tenth year, PDSI values in the eleventh, twelfth, thirteenth, fourteenth and fifteenth years would be used in equation (2), producing five ΔGPP values. The mean annual ΔC per pixel after severe droughts and fires is presented in Fig. 4a,c, indicating a reduction in carbon assimilation through photosynthesis due to disturbances.

In warming scenarios, we utilized 4 km monthly precipitation and PET data under +2 °C warming obtained from ref. 46 to generate PDSI values under the +2 °C scenario with the '`scPDSI`' package in R. The precipitation and PET data under the +2 °C scenario corresponded to the nominal years of 1985–2015. Monthly PDSI values under the warming scenario were calculated and averaged to the annual level. The change in carbon uptake was estimated using the annual PDSI values under the warming scenario following the same approach outlined in equation (2), with Δk and Δb obtained from Fig. 1 and Extended Data Fig. 3, respectively. The mean annual ΔC under the warming scenario is depicted in Fig. 4.

Caveats

The GPP products used in this study are based on different inputs and models, leading to inherent differences in results when comparing across different GPP datasets. To increase the robustness of our analysis, we used a detrended, ensemble mean approach when deriving GPP for our study. Although we believe that taking an ensemble mean strengthens the analysis above any based on a single product alone, caution should be exercised in interpretation of remote-sensing-based GPP data, which tend to overestimate vegetation productivity in droughts (particularly severe droughts⁴⁷). To overcome the drought limitation in this study, we used pre-drought and post-drought GPP data to conduct regression analysis, rather than data during drought. This approach avoids the potential limitations of GPP overestimation in droughts. Finally, our method used to estimate the impacts of drought sensitivity change on carbon uptake could induce uncertainties, particularly under warming scenarios, because other factors such as plant acclimation and climate change were not considered (but are currently poorly constrained in the literature).

Ethics and inclusion statement

This research involves collaborations of scientists in both the USA and Spain. All authors contributed to the study design, analysis and results, and their names are listed on the title page. All data are publicly available from online resources. This is a continental-scale study and no local partners or agencies are required. The authors agreed on the roles and responsibilities related to this study. This research is not restricted or prohibited in the setting of the researchers. No animals, discrimination, health issues or biological materials are relevant to this research.

Reporting summary

Further information on research design is available in the Nature Portfolio Reporting Summary linked to this article.

Data availability

The NTSG Landsat GPP data were obtained from Google Earth Engine: <https://developers.google.com/earth-engine/datasets/catalog>. The GLASS GPP data were obtained from <http://www.glass.umd.edu/Download.html>. The EC-LUE GPP data were obtained from <https://doi.org/10.6084/m9.figshare.8942336.v3>. The NIRv GPP data were downloaded from <https://doi.org/10.6084/m9.figshare.12981977.v2>. The FLUXNET2015 GPP dataset is available at <https://fluxnet.org/data/fluxnet2015-dataset/>. The historical climatic data (for example, precipitation) and PDSI data were obtained from TerraClimate (<https://www.climatologylab.org/terraclimate.html>). The climatic data under +2 °C warming scenario were also obtained from TerraClimate (<https://www.climatologylab.org/terraclimate.html>). The MTBS maps of fire severity are available at <https://www.mtbs.gov/direct-download>. The land-cover maps were obtained from Earthdata (<https://lpdaac.usgs.gov/products/mcd12q1v006/>). The mean annual rates of mortality were from ref. 11, and no new mortality data were produced. The US boundary was from DATA.GOV (<https://data.gov/>). The data produced in this study are available via Figshare (<https://doi.org/10.6084/m9.figshare.23730507>)⁴⁸.

Code availability

All analysis was done in the open-source software R. The code is available via Figshare (<https://doi.org/10.6084/m9.figshare.23730507>)⁴⁸.

References

35. Robinson, N. P. et al. Terrestrial primary production for the conterminous United States derived from Landsat 30 m and MODIS 250 m. *Remote Sens. Ecol. Conserv.* **4**, 264–280 (2018).
36. Liang, S. et al. The Global Land Surface Satellite (GLASS) product suite. *Bull. Am. Meteorol. Soc.* **102**, E323–E337 (2021).
37. Zheng, Y. et al. Improved estimate of global gross primary production for reproducing its long-term variation, 1982–2017. *Earth Syst. Sci. Data* **12**, 2725–2746 (2020).
38. Wang, S., Zhang, Y., Ju, W., Qiu, B. & Zhang, Z. Tracking the seasonal and inter-annual variations of global gross primary production during last four decades using satellite near-infrared reflectance data. *Sci. Total Environ.* **755**, 142569 (2020).
39. Wells, N., Goddard, S. & Hayes, M. J. A self-calibrating Palmer Drought Severity Index. *J. Clim.* **17**, 2335–2351 (2004).
40. Abatzoglou, J. T., Dobrowski, S. Z., Parks, S. A. & Hegewisch, K. C. TerraClimate, a high-resolution global dataset of monthly climate and climatic water balance from 1958–2015. *Sci. Data* **5**, 170191 (2018).
41. van der Schrier, G., Barichivich, J., Briffa, K. R. & Jones, P. D. A scPDSI-based global data set of dry and wet spells for 1901–2009. *J. Geophys. Res. Atmos.* **118**, 4025–4048 (2013).
42. Aitken, A. C. On least squares and linear combination of observations. *Proc. R. Soc. Edinb.* **55**, 42–48 (1936).
43. Breiman, L. Random Forests. *Mach. Learn.* **45**, 5–32 (2001).
44. Cao, S. et al. Spatiotemporally consistent global dataset of the GIMMS Leaf Area Index (GIMMS LAI4g) from 1982 to 2020. *Earth Syst. Sci. Data* **15**, 4877–4899 (2023).
45. Cheng, W. et al. Global monthly gridded atmospheric carbon dioxide concentrations under the historical and future scenarios. *Sci. Data* **9**, 83 (2022).
46. Qin, Y. et al. Agricultural risks from changing snowmelt. *Nat. Clim. Change* **10**, 459–465 (2020).
47. Stocker, B. D. et al. Drought impacts on terrestrial primary production underestimated by satellite monitoring. *Nat. Geosci.* **12**, 264–270 (2019).
48. Liu, M. et al. Forest sensitivity change in response to disturbances. *Figshare* <https://doi.org/10.6084/m9.figshare.23730507> (2023).

Acknowledgements

The study was supported by the Wilkes Center at the University of Utah, and thanks to the Anderegg lab. J.P. was supported by the TED2021-132627B-I00 grant, funded by MCIN and the European Union NextGeneration EU/PRTR, and the CIVP20A6621 grant funded by the Fundación Ramón Areces. A.T.T. acknowledges funding from National Science Foundation grants 2003205, 2017949 and 2216855, the University of California Laboratory Fees Research Program award no. LFR-20-652467 and the Gordon and Betty Moore Foundation grant GBMF11974. W.R.L.A. acknowledges support from the David and Lucile Packard Foundation and US National Science Foundation grants 1802880, 2003017 and 2044937 as well as the Alan T. Waterman award IOS-2325700.

Author contributions

M.L. and W.R.L.A. conceptualized and designed the study with input from all co-authors. M.L. performed the analysis. M.L. wrote the initial draft and A.T.T., J.P. and W.R.L.A. discussed the design, analyses and results and provided extensive and valuable comments and revisions.

Competing interests

The authors declare no competing interests.

Additional information

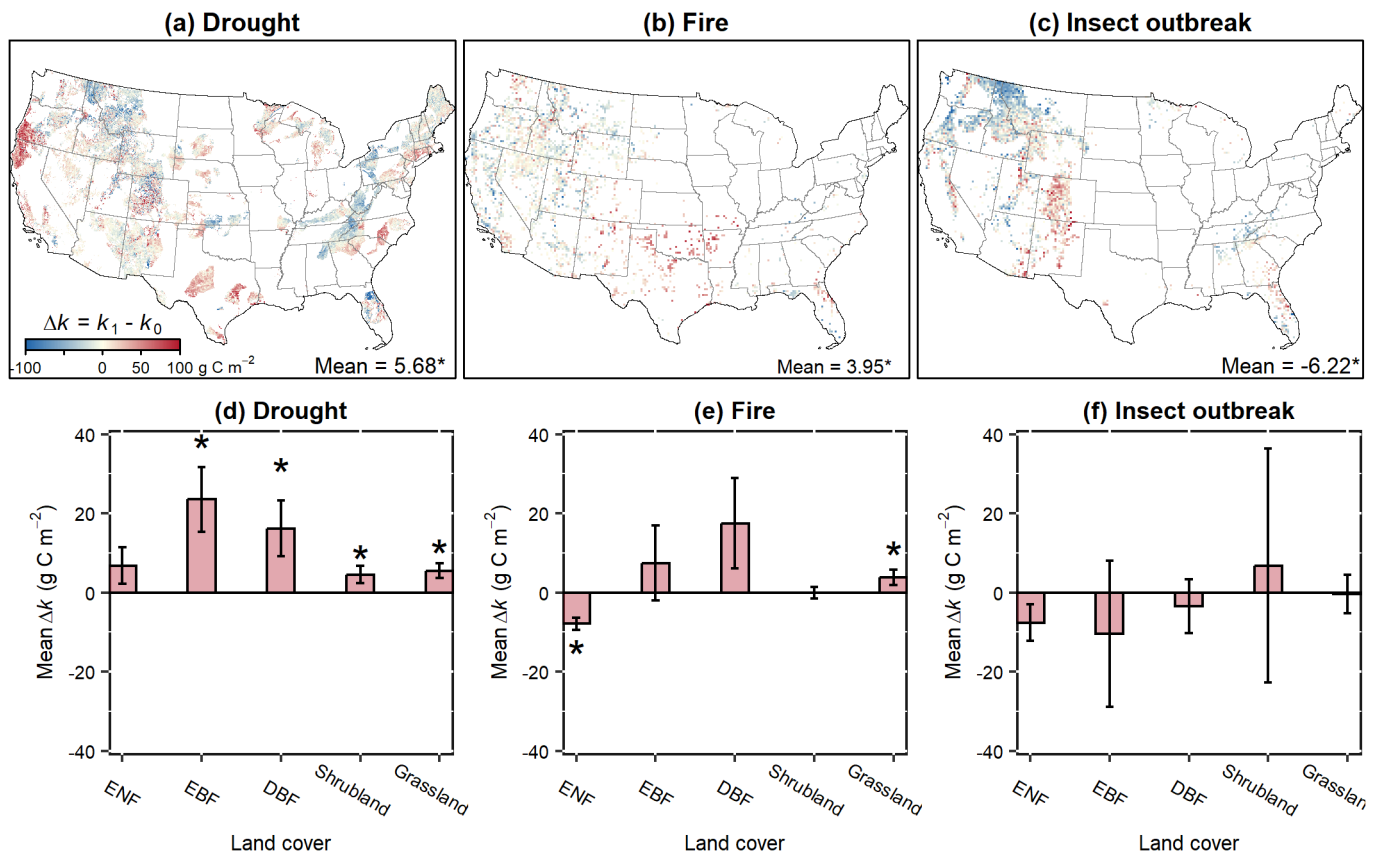
Extended data is available for this paper at <https://doi.org/10.1038/s41558-024-02022-1>.

Supplementary information The online version contains supplementary material available at <https://doi.org/10.1038/s41558-024-02022-1>.

Correspondence and requests for materials should be addressed to Meng Liu.

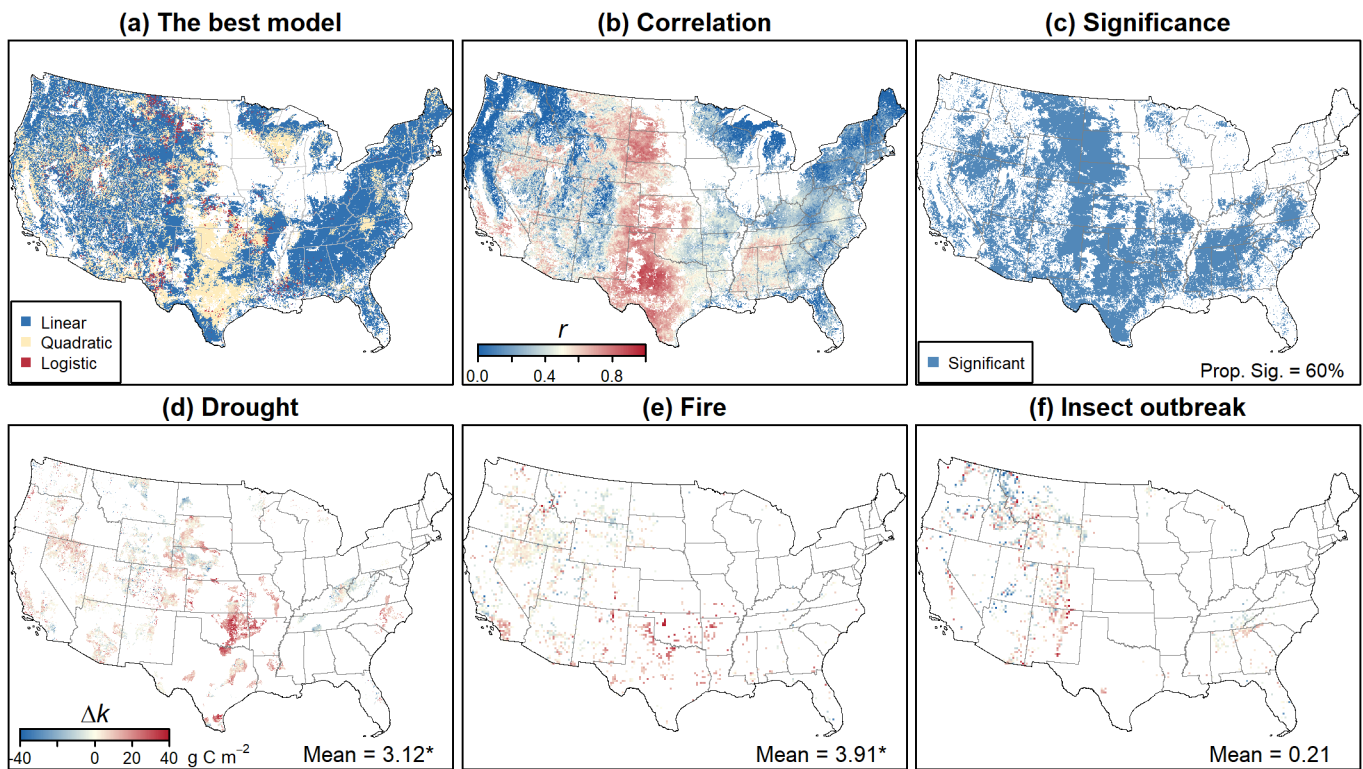
Peer review information *Nature Climate Change* thanks Steven Running, Dominik Thom and the other, anonymous, reviewer(s) for their contribution to the peer review of this work.

Reprints and permissions information is available at www.nature.com/reprints.



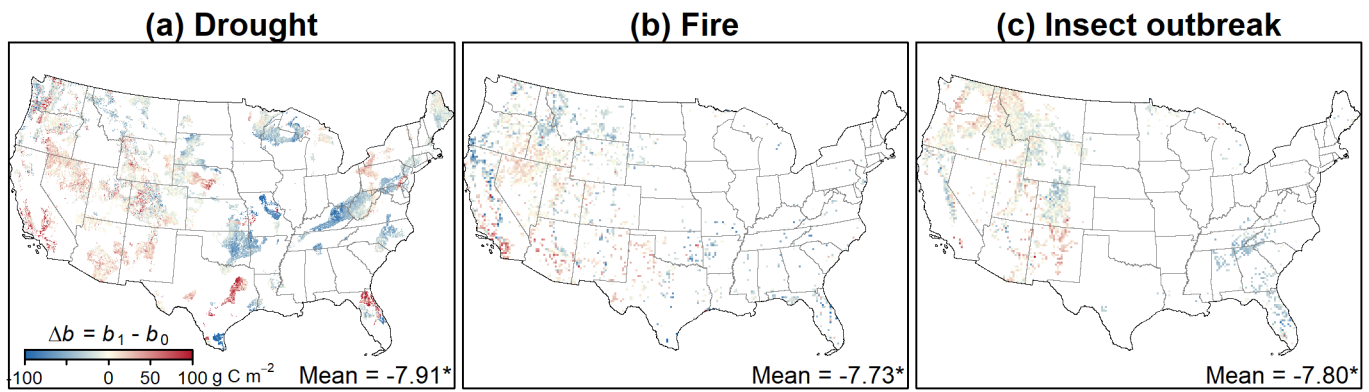
Extended Data Fig. 1 | The drought sensitivity increased significantly after severe droughts and fires when using SPEI to represent water stress. (a–c) The change in sensitivity across CONUS after severe (a) droughts, (b) fires, and (c) insect outbreaks. The resolution of the distribution maps for fires and insect outbreaks was aggregated to 20 km for visual display. (d–f) The change in sensitivity among different land-cover types after severe (d) droughts (left to

right, $N=2668, 490, 5521, 1450, 8720$), (e) fires ($N=1944, 178, 258, 601, 6068$), and (f) insect outbreaks ($N=7320, 111, 548, 157, 3904$). The error bars are standard errors. Asterisks indicate significance at the 0.05 level (two-sided) based on the GLS model. Multiple comparisons are not applicable. Definitions of disturbances for a pixel: droughts, $\text{SPEI} < -1.2$ ($\text{PDSI} < -3$); fires, the proportion of burned area $> 10\%$; insect outbreaks, insect caused mortality $> 0.03\%$.



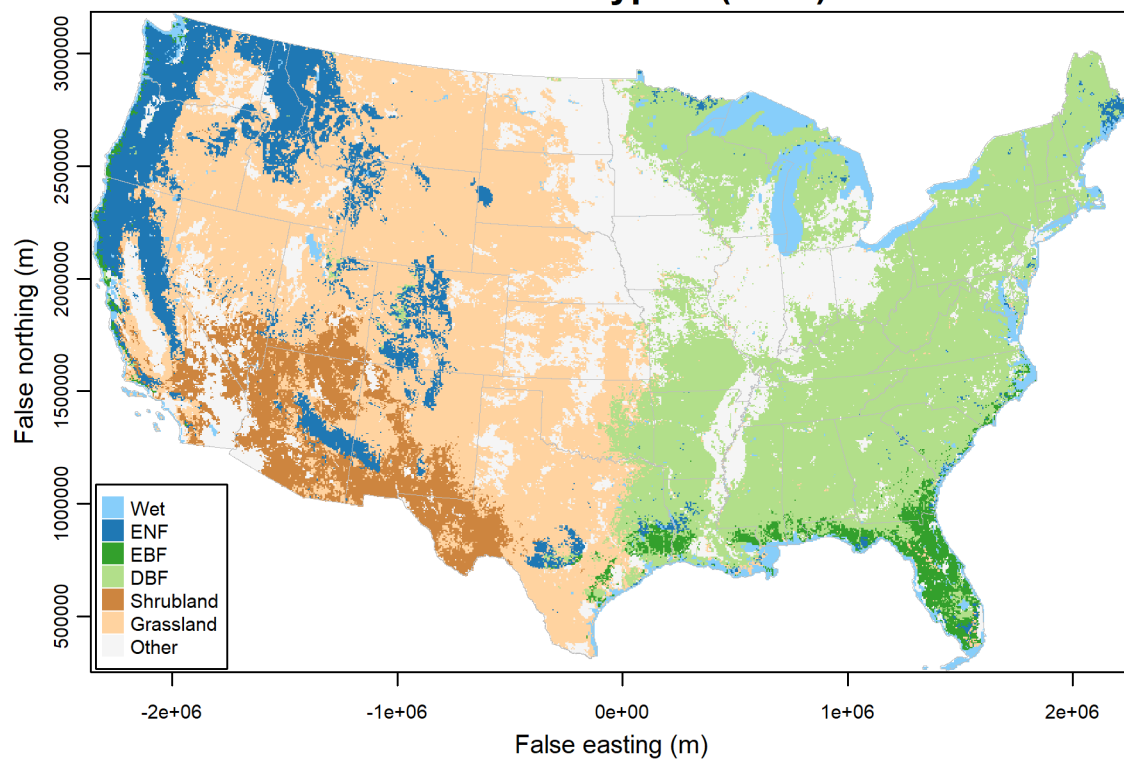
Extended Data Fig. 2 | The best model for each pixel across CONUS. a There are three models employed: linear (blue), quadratic (yellow), and logistic (red) models. The best model is defined as the one with the minimum Akaike Information Criterion (AIC). The linear model is the best for 69% of pixels across CONUS. b-c The (b) correlation between GPP anomaly and PDSI and (c) the

corresponding significance ($p < 0.05$, two-sided t test). 60% of the available pixels present significant correlations between GPP anomaly and PDSI. d-f The change in sensitivity (Δk) for severe (d) droughts, (e) fires, and (f) insect outbreaks using the significant pixels in panel c. The results are comparable to those using all available pixels shown in Fig. 1.

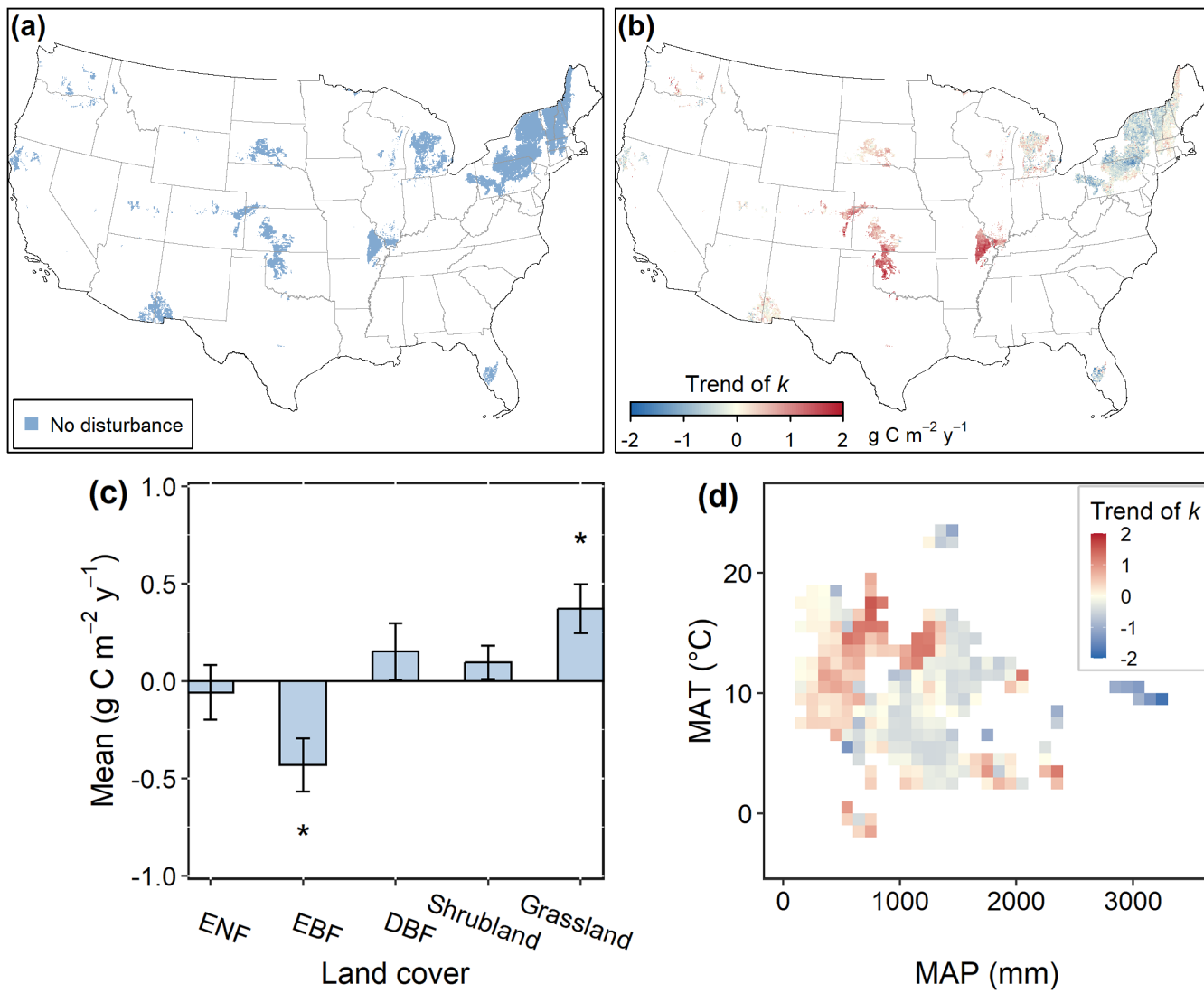


Extended Data Fig. 3 | The intercept of the GPP-PDSI model decreased significantly after severe disturbances. (a–c) The changes in the intercept (Δb) across CONUS after severe (a) droughts, (b) fires, and (c) insect outbreaks. The

resolution of the distribution maps for fires and insect outbreaks was aggregated to 20 km for visual display. Asterisks indicate significance at the 0.05 level (two-sided) based on the GLS model.

MCD12Q1 Type 5 (2001)

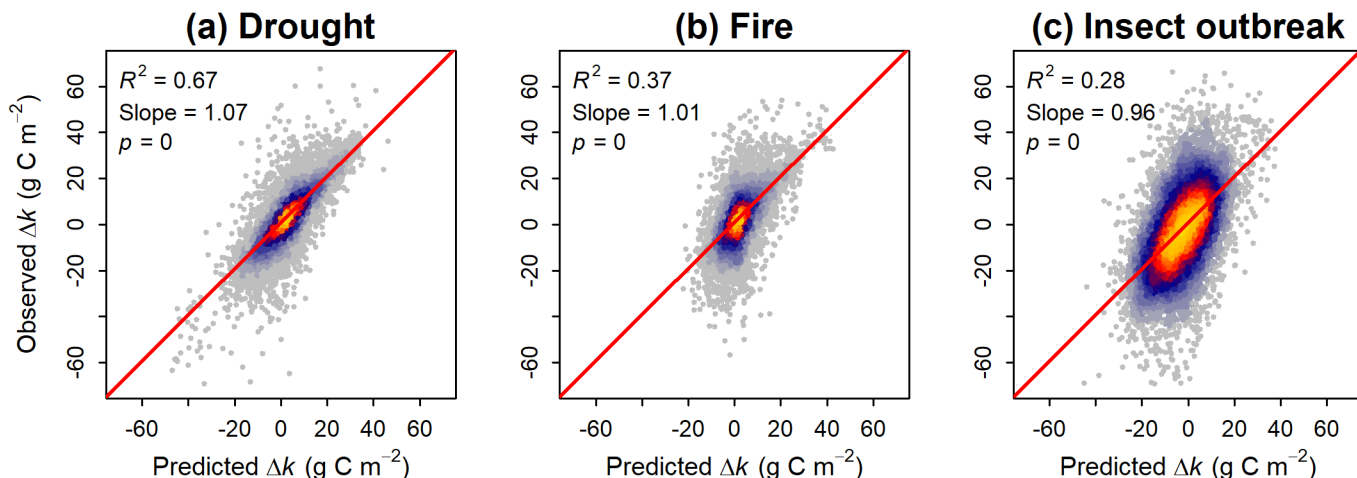
Extended Data Fig. 4 | Land-cover map from the MCD12Q1 Type 5 classification in 2001. ENF, evergreen needleleaf forest; EBF, evergreen broadleaf forest; and DBF, deciduous broadleaf forest.



Extended Data Fig. 5 | Changes in drought sensitivity in undisturbed regions.

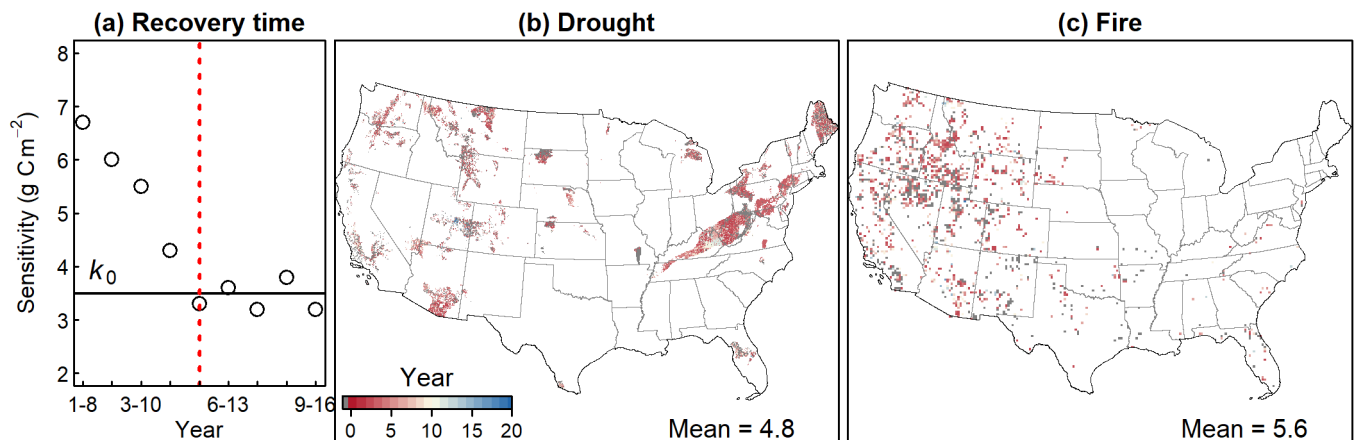
(a) The distribution of undisturbed regions in 1982–2018. (b) The trend of sensitivity (k) in undisturbed regions, where the trend was derived using an eight-year moving window, with k calculated for each window. The trend of sensitivity (Trend of k) is the slope of sensitivity vs year. (c) The mean trend of sensitivity for

the land-cover types (left to right, $N=258, 99, 2344, 228, 980$), where the asterisks indicate significance ($p = 0.002$ and 0.003 , respectively, two-sided) based on the GLS model. The error bars are standard errors. Multiple comparisons are not applicable. (d) The distribution of the trend of sensitivity (Trend of k) in climate space (mean annual temperature (MAT) vs mean annual precipitation (MAP)).



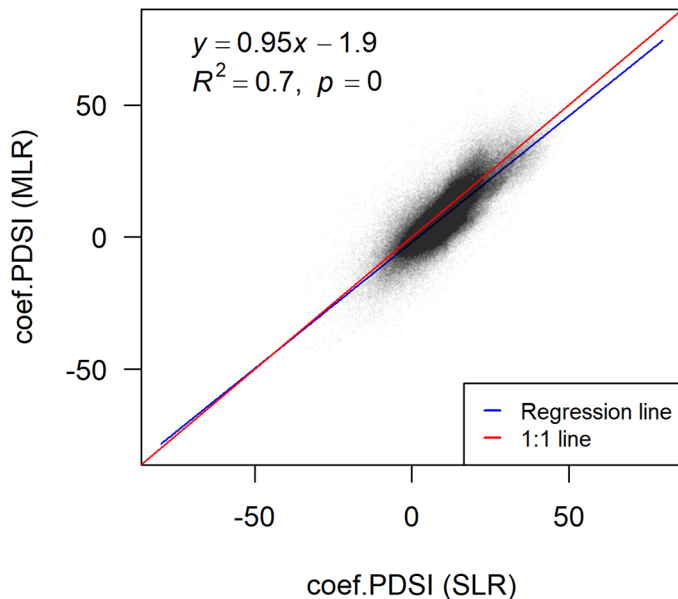
Extended Data Fig. 6 | Correlation of the observed change in sensitivity and the Random Forest model estimated change in sensitivity. (a–c) The scatterplots for severe (a) droughts, (b) fires, and (c) insect outbreaks. The red

lines are the $y = x$ lines, and orange color indicates high point density. The R^2 , slope, and p values (two-sided t test) are from linear regression: observed vs predicted Δk . Multiple comparisons are not applicable.

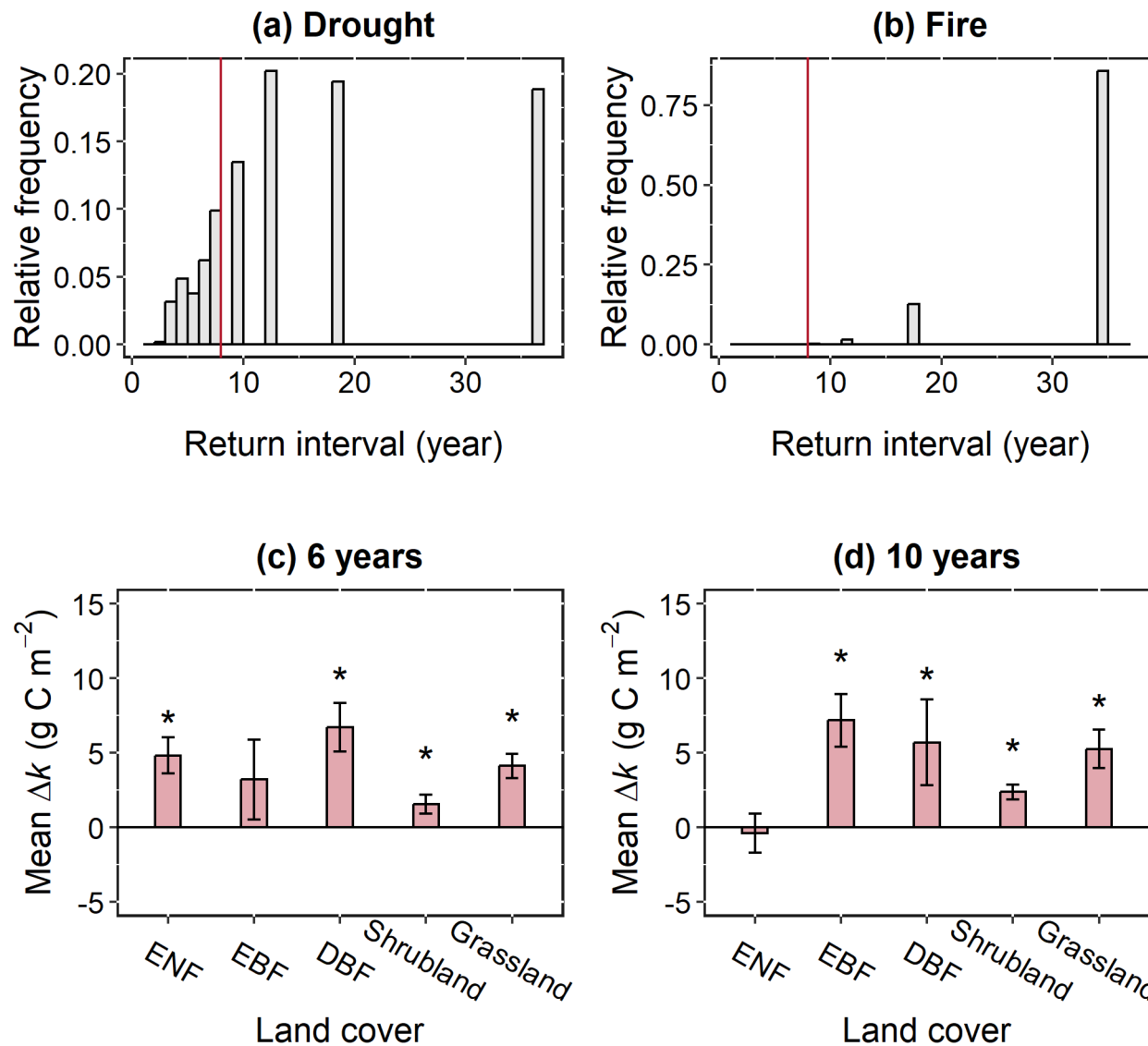


Extended Data Fig. 7 | Recovery time for the sensitivity to revert to its pre-disturbance level. (a) A schematic to illustrate the definition of recovery time, where each circle means the sensitivity in an eight-year moving window, and the red dotted line indicates the identified recovery time (that is 5 years post-disturbance). (b–c) The distribution of recovery time derived from pixels with

long post-disturbance time for severe (b) droughts and (c) fires. Pixels never recovered (gray color; ~30% of pixels) are removed when calculating the mean recovery time. The resolution of the distribution map for fire was aggregated to 20 km for visual display.

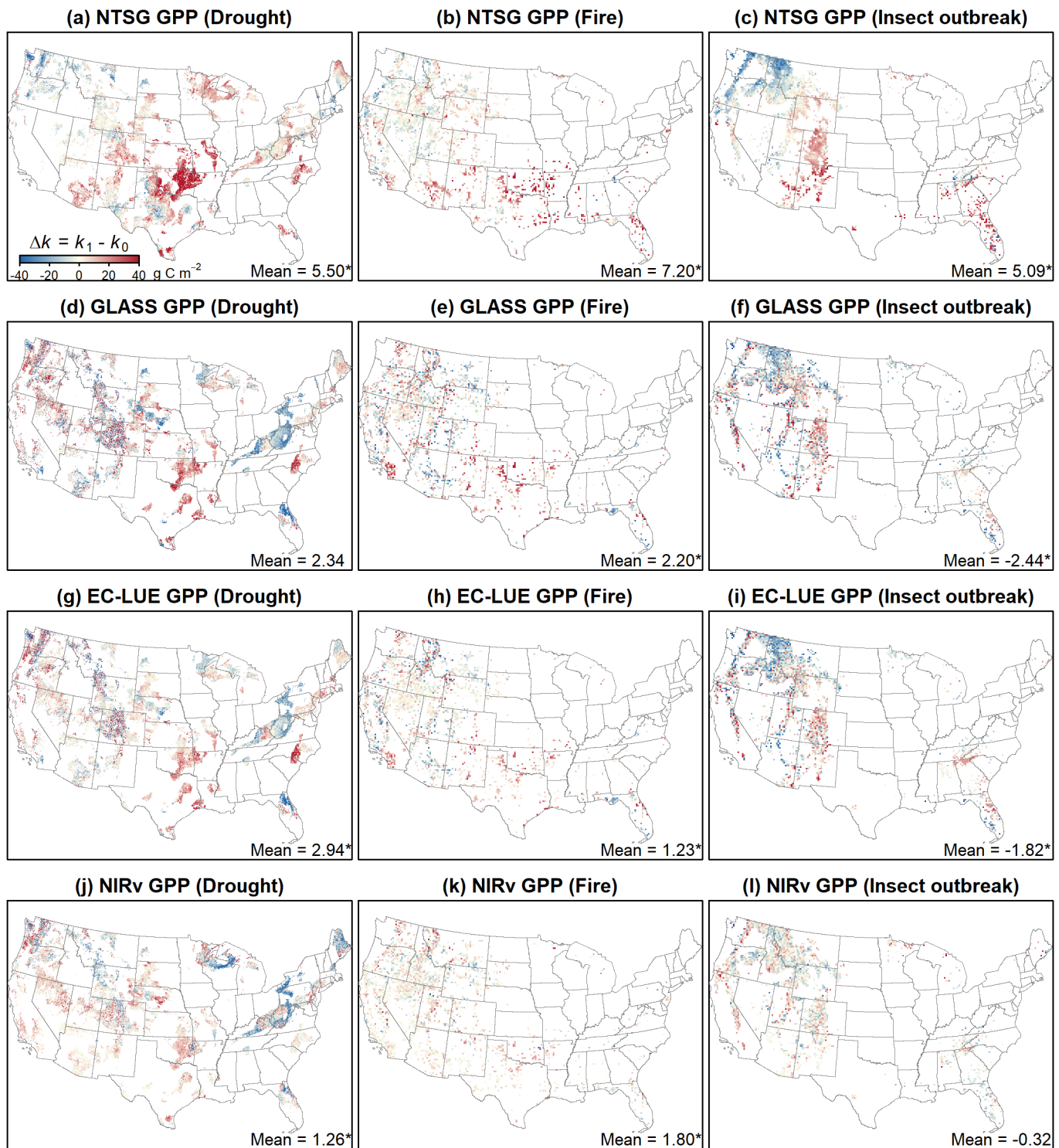


Extended Data Fig. 8 | Comparison of coefficients (sensitivity) of PDSI from different models. Simple linear regression (SLR: $\text{GPP}_{\text{anomaly}} \sim \text{PDSI}$) and multiple linear regression (MLR: $\text{GPP}_{\text{anomaly}} \sim \text{Srad}_{\text{anomaly}} + \text{T}_{\text{anomaly}} + \text{SM}_{\text{anomaly}} + \text{PDSI}$) are used based on data from 1982 to 2018. Each point in the figure indicates a pixel. The p value is from two-sided t test, and multiple comparisons are not applicable.



Extended Data Fig. 9 | Comparisons of drought and fire return intervals and different thresholds as the minimum number of years for regression.
(a–b) The histograms of return intervals of severe (a) droughts and (b) fires in CONUS, where the bin width is one year. The red lines indicate return intervals of eight years. (c–d) The change in sensitivity when using (c) six years (left to right,

$N=3336, 591, 8500, 2012, 12744$) and (d) ten years ($N=1847, 228, 4167, 886, 4831$) as the minimum for regression. The error bars are standard errors. Asterisks indicate significance at the 0.05 level (two-sided) when using the GLS model. Multiple comparisons are not applicable.



Extended Data Fig. 10 | Changes in drought sensitivity using the four remotely sensed GPP products (NTSG, GLASS, EC-LUE and NIRv GPP) separately with PDSI representing water stress. The asterisks indicate $p < 0.05$ (two-sided) based on the GLS model.

Reporting Summary

Nature Portfolio wishes to improve the reproducibility of the work that we publish. This form provides structure for consistency and transparency in reporting. For further information on Nature Portfolio policies, see our [Editorial Policies](#) and the [Editorial Policy Checklist](#).

Statistics

For all statistical analyses, confirm that the following items are present in the figure legend, table legend, main text, or Methods section.

n/a Confirmed

The exact sample size (n) for each experimental group/condition, given as a discrete number and unit of measurement

A statement on whether measurements were taken from distinct samples or whether the same sample was measured repeatedly

The statistical test(s) used AND whether they are one- or two-sided
Only common tests should be described solely by name; describe more complex techniques in the Methods section.

A description of all covariates tested

A description of any assumptions or corrections, such as tests of normality and adjustment for multiple comparisons

A full description of the statistical parameters including central tendency (e.g. means) or other basic estimates (e.g. regression coefficient) AND variation (e.g. standard deviation) or associated estimates of uncertainty (e.g. confidence intervals)

For null hypothesis testing, the test statistic (e.g. F , t , r) with confidence intervals, effect sizes, degrees of freedom and P value noted
Give P values as exact values whenever suitable.

For Bayesian analysis, information on the choice of priors and Markov chain Monte Carlo settings

For hierarchical and complex designs, identification of the appropriate level for tests and full reporting of outcomes

Estimates of effect sizes (e.g. Cohen's d , Pearson's r), indicating how they were calculated

Our web collection on [statistics for biologists](#) contains articles on many of the points above.

Software and code

Policy information about [availability of computer code](#)

Data collection All data were collected and processed with R version 4.1.3. The DATA AVAILABILITY statement was added.

Data analysis All data were analyzed with R version 4.1.3. The code is available from figshare: <https://figshare.com/s/ace0046a5200b4451e82>

For manuscripts utilizing custom algorithms or software that are central to the research but not yet described in published literature, software must be made available to editors and reviewers. We strongly encourage code deposition in a community repository (e.g. GitHub). See the Nature Portfolio [guidelines for submitting code & software](#) for further information.

Data

Policy information about [availability of data](#)

All manuscripts must include a [data availability statement](#). This statement should provide the following information, where applicable:

- Accession codes, unique identifiers, or web links for publicly available datasets
- A description of any restrictions on data availability
- For clinical datasets or third party data, please ensure that the statement adheres to our [policy](#)

The NTSG Landsat GPP data were obtained from the Google Earth Engine: <https://developers.google.com/earth-engine/datasets/catalog>. The GLASS GPP data were obtained from <http://www.glass.umd.edu/Download.html>. The EC-LUE GPP data were obtained from <https://doi.org/10.6084/m9.figshare.8942336.v3>. The NIRv GPP data were downloaded from <https://doi.org/10.6084/m9.figshare.12981977.v2>. The FLUXNET2015 GPP data set is available at <https://fluxnet.org/data/fluxnet2015-dataset/>. The historical climatic data (e.g. precipitation) and PDSI data were obtained from TerraClimate (<https://www.climatologylab.org/>)

Human research participants

Policy information about [studies involving human research participants](#) and [Sex and Gender in Research](#).

Reporting on sex and gender	This study didn't involve sex or gender-related data.
Population characteristics	This study didn't involve human research participants or human-related data.
Recruitment	This study didn't involve human research participants or human-related data.
Ethics oversight	This study didn't involve human research participants or human-related data.

Note that full information on the approval of the study protocol must also be provided in the manuscript.

Field-specific reporting

Please select the one below that is the best fit for your research. If you are not sure, read the appropriate sections before making your selection.

Life sciences Behavioural & social sciences Ecological, evolutionary & environmental sciences

For a reference copy of the document with all sections, see nature.com/documents/nr-reporting-summary-flat.pdf

Ecological, evolutionary & environmental sciences study design

All studies must disclose on these points even when the disclosure is negative.

Study description	This study quantified the change in the sensitivity of ecosystem gross primary production (GPP) to drought stress (water availability) before and after severe droughts, fires, and insect outbreaks. Leveraging long-term remotely sensed GPP data in the conterminous United States (CONUS), we performed regression analysis to understand the response of GPP to variations in drought stress, as indicated by widely used drought indices like the Palmer Drought Severity Index (PDSI) and the Standardized Precipitation–Evapotranspiration Index (SPEI). We calculated the sensitivity of GPP to drought stress (referred to as "drought sensitivity") and compared it before and after disturbances. Machine learning models, specifically Random Forest regression, were employed to uncover the drivers and potential mechanisms underlying changes in drought sensitivity. We further estimated the potential carbon uptake change in response to the drought sensitivity change. Results indicate that the sensitivity of GPP to subsequent drought stress increased significantly after initial drought and fire disturbances in CONUS and decreased after insect outbreak events. Decreases in soil moisture, high mean annual temperature, and hot and dry environments were major environmental drivers associated with increased sensitivity. Due to the increased sensitivity, estimated carbon uptake decreased markedly under future warming scenarios.
Research sample	We focused on ecosystem drought sensitivity change in the conterminous United States because this region is vulnerable to climate-driven disturbances, such as droughts and wildfires. This study used four remotely sensed GPP products (NTSG GPP, GLASS GPP, EC-LUE GPP, and NIRv GPP) and two widely recognized drought indices (PDSI and SPEI) to represent ecosystem productivity and drought stress, respectively.
Sampling strategy	We used all available samples, i.e. pixels, to conduct the analysis.
Data collection	All data (GPP and drought indices) are publicly available from online resources, which were provided in the Data availability statement. Meng Liu obtained these data and processed them with R.
Timing and spatial scale	Annual GPP data and drought indices (PDSI and SPEI) in 1982–2018 across the conterminous United States were used to demonstrate the long-term dynamics of drought sensitivity change. We focused on long-term changes in the sensitivity of forest GPP to drought stress at a large scale.
Data exclusions	No data were excluded. We used all available samples, i.e. pixels, to conduct the analysis.
Reproducibility	All attempts to repeat the experiment, i.e. calculating the sensitivity of GPP to drought stress, were successful.
Randomization	The samples were not allocated randomly in this study. Samples used to derive the sensitivity change were separated by the year when the disturbances occurred. For a disturbance like drought, pre-drought and post-drought data were separated by the drought year and leveraged to calculate pre-drought sensitivity and post-drought sensitivity, respectively. The sensitivity change was the difference between post-drought and pre-drought sensitivity.
Blinding	Blinding is not relevant to this study.

Reporting for specific materials, systems and methods

We require information from authors about some types of materials, experimental systems and methods used in many studies. Here, indicate whether each material, system or method listed is relevant to your study. If you are not sure if a list item applies to your research, read the appropriate section before selecting a response.

Materials & experimental systems

n/a	Involved in the study
<input checked="" type="checkbox"/>	Antibodies
<input checked="" type="checkbox"/>	Eukaryotic cell lines
<input checked="" type="checkbox"/>	Palaeontology and archaeology
<input checked="" type="checkbox"/>	Animals and other organisms
<input checked="" type="checkbox"/>	Clinical data
<input checked="" type="checkbox"/>	Dual use research of concern

Methods

n/a	Involved in the study
<input checked="" type="checkbox"/>	ChIP-seq
<input checked="" type="checkbox"/>	Flow cytometry
<input checked="" type="checkbox"/>	MRI-based neuroimaging